

Taylor & Francis
Taylor & Francis Group

Materials Science and Technology

ISSN: (Print) (Online) Journal homepage: https://www.tandfonline.com/loi/ymst20

Effect of ball-burnishing on surface integrity and fatigue behaviour of 7175-T6 AA

Melika Ozer, Kübra Dalli & Alpay Ozer

To cite this article: Melika Ozer, Kübra Dalli & Alpay Ozer (2022): Effect of ball-burnishing on surface integrity and fatigue behaviour of 7175-T6 AA, Materials Science and Technology, DOI: 10.1080/02670836.2022.2142744

To link to this article: https://doi.org/10.1080/02670836.2022.2142744

Published online: 06 Nov 2022.

Submit your article to this journal

Article views: 63

View related articles

View Crossmark data

Full Terms & Conditions of access and use can be found at
https://www.tandfonline.com/action/journalInformation?journalCode=ymst20

MATERIALS SCIENCE AND TECHNOLOGY
https://doi.org/10.1080/02670836.2022.2142744

Check for updates

Effect of ball-burnishing on surface integrity and fatigue behaviour of 7175-T6 AA

Melika Ozer [a], Kübra Dalli [b] and Alpay Ozer [c]

[a]Metallurgical and Materials Engineering, Faculty of Technology, Gazi University, Ankara, Turkey; [b]Metallurgical and Materials Engineering, Institute of Science, Gazi University, Ankara, Turkey; [c]Vocational School of Technical Sciences, Gazi University, Ankara, Turkey

ABSTRACT

The burnishing process was performed using different feed rates, rotational speed and penetration depth parameters to alloy Al 7175-T6. Surface roughness, fatigue life and hardness of the samples were determined. Microstructural examinations of the samples were performed. In the surface roughness measurements, occurred a linear increase in proportion to the increasing feed rate. The increase in the penetration depth affected negatively the surface roughness. Significant increases were acquired in the fatigue life of the burnished samples. The hardness values of the burnishing samples are higher than the hardness value of the base material. The rotational movement of the steel ball during the burnishing process were been caused the aspect ratio of the grains in the microstructure to change.

ARTICLE HISTORY
Received 7 June 2022
Revised 22 September 2022
Accepted 27 October 2022

KEYWORDS
Al 7175; burnishing; fatigue life; microstructure

Introduction

The use of thermal, mechanical, thermo-mechanical or thermo-chemical surface strengthening techniques has attracted the interest of researchers intensely since the early twentieth century to improve the surface integrity of materials [1,2].

In general, the state of the surface layer in terms of microstructure, residual stresses, microhardness and roughness is very important for the fatigue strength and fatigue life [3,4]. Various surface treatment techniques have been developed to obtain a good surface quality and to improve the mechanical properties of the material. Grinding, shot peening and controlled surface rolling (burnishing) are methods of mechanical surface treatment [5–8]. Among these techniques, the burnishing process has attracted attention in recent years [9,10]. Burnishing is a cold deformation technique performed by crushing the surfaces of materials without removing chips [11–15]. This technique creates residual compression stresses on the surface of the material and affects the microstructure [16–18]. Thus, while the fatigue life and wear resistance of the material are improved, stress corrosion cracking is delayed [19–25]. Especially in aluminium alloys, surface plastic deformation increases the fatigue life a significantly [26]. In recent years, the burnishing process has been applied to a wide range of materials such as iron-based alloys, brass and aluminium [27,28]. Defined as the metal of the twenty-first century, aluminium alloys are ideal for many engineering applications due to their promising properties and are among the sought-after material systems especially in aircraft and automobile industry applications [10,29,30]. Particularly, 7xxx series alloys are the preferred Al series material group in the automotive and aerospace industries due to their high specific strength, high fracture toughness, excellent anti-fatigue and resistance to stress corrosion cracking. 7175 Al alloy, on the other hand, is one of the leading alloys of the 7xxx series and is defined as a high-strength aluminium alloy and has intensive use in the aerospace and automotive industries [31–33]. FSW and ball-burnishing processes are combined in 2050 Al alloy. The results showed that the ball-burnishing process increased the material hardness by approximately 37.5% and improved the surface properties by reducing the surface roughness from 2.23 to 0.6 µm. In addition, it was stated that high compressive residual stresses occurred in the samples [34,35].

The aim of this study is to improve the fatigue performance of high-strength Al 7175-T6 alloy, which is often called aerospace alloys due to its wide applications in the aerospace industry, by burnishing surface treatment. Fatigue behaviour of materials is closely related to surface integrity. For this reason, the effects of the burnishing treatment applied to the Al 7175-T6 test material on the surface roughness (Ra), fatigue life, microhardness and microstructure were investigated by using different parameters.

CONTACT Melika Ozer mcerah@gazi.edu.tr Metallurgical and Materials Engineering, Faculty of Technology, Gazi University, 06560 Ankara, Turkey

© 2022 Institute of Materials, Minerals and Mining.

Table 1. Chemical composition and mechanical properties of the EN AW Al 7175-T6 material.

	Chemical composition (wt-%)								
EN AW Al 70175-T6	Si	Fe	Cu	Mn	Mg	Cr	Zn	Ti	Al
	0.18	0.33	1.37	0.4	2.43	0.21	5.38	0.024	Bal.

	Mechanical properties				
	$Rp_{0.2}$ (MPa)	Rm (MPa)	Shear Strength (MPa)	Elongation (%)	Modulus of elasticity (GPa)
	501	582	300	9,6	72

Table 2. Burnishing process parameters.

Sample code	Penetration depth (mm)	Feed rate (mm rev^{-1})	Rotational speed (rev min^{-1})
0.10/0.15/100	0.10	0.15	100
0.10/0.30/100	0.10	0.30	100
0.10/0.60/100	0.10	0.60	100
0.10/0.15/200	0.10	0.15	200
0.10/0.30/200	0.10	0.30	200
0.10/0.60/200	0.10	0.60	200
0.15/0.15/200	0.15	0.15	200
0.15/0.30/200	0.15	0.30	200
0.15/0.60/200	0.15	0.60	200
0.05/0.60/400	0.05	0.60	400
0.10/0.15/400	0.10	0.15	400
0.10/0.30/400	0.10	0.30	400
0.10/0.60/400	0.10	0.60	400
0.15/0.60/400	0.15	0.60	400

Experimental procedure

Material

In this study, semi-finished EN AW Al 7175-T6 alloy with dimensions of 4 × 350 × 400 mm was used as test material. The chemical composition and mechanical properties of the EN AW Al 7175-T6 alloy are given in Table 1.

Method

Al 7175-T6 alloy with dimensions of 4 × 350 × 400 mm was subjected to the ball-burnishing process using the parameters given in Table 2. The burnishing processes were carried out using a computer numeric controlled (CNC) mechanical vertical machining centre. A steel ball with a diameter of 15.9 mm made of AISI 4340 material was used as the deforming element (Figure 1).

After the burnishing process, the roughness values of the rolling traces formed on the plates were measured as Ra. Surface roughnesses were carried out by using Mitutoyo/SJ-210 brand/model device according to ISO 4287:1997 standard. Five measurements were taken for one experimental point. The arithmetic average of five measurements was taken. The measuring range was performed in Auto mode.

Standard metallographic grinding and polishing processes were applied to the samples for microstructure analysis. The samples were etched using Keller's etching. Microstructure studies were performed with a Leica DMI 5000M optical microscope and Jeol JSM 6060 LV scanning electron microscope (SEM).

In order to determine the effect of burnishing on fatigue strength, bending fatigue test specimens were prepared according to DIN 50142 and fatigue tests were carried out. In Figure 2, fatigue test sample and fatigue test device image are given. A conventional fatigue testing machine in compliance with DIN 50142 was used, which allows dynamic fatigue tests of samples made of non-ferrous metals and steels. The electro-mechanical conventional fatigue testing machine developed using a linear engine and having a Programmable Logic Controller (PLC) system has been patented with the patent number TR 2016/13535. Fatigue tests were performed at room temperature, sinusoidal cyclic push–pull loading (stress ratio $R = -1$) at a constant amplitude of approximately 300 Hz according to DIN 50142. The mean stress is set to zero. Wöhler curves were formed graphically with the data obtained from the experiments. The number of cycles corresponding to the highest value in these curves was obtained by plotting logarithmically. $N = 2 \times 10^6$ value used in scientific studies was used as the limit cycle number (life time) in bending fatigue tests. Fatigue test specimens were fixed to the test device from the upper and lower surfaces perpendicular to the A_1 section shown in Figure 2(c). Depending on the specimen form, fractures are expected to occur in the A_2 section (Figure 2(c)). For this reason, the stress amplitudes that the applied test forces will create in the A_2 section were calculated. Calculations were performed using Formula 3 derived from Formulas 1 and 2. The stress value corresponding to approximately 90% of the yield stress ($Rp_{0.2}$) of the Al 7175-T6 alloy was taken as the highest stress value.

$$\sigma = \frac{MC}{\mathrm{I}} \tag{1}$$

$$I = \frac{Bh^3}{12} \tag{2}$$

$$\sigma = \frac{6FL}{Bh^2} \tag{3}$$

where σ is the bending stress in MPa, M is the bending moment, F is the bending force in kg, L is the moment arm length in mm, C is the distance from neutral axis ($h/2$), B is the horizontal width (mm), h is the thickness in mm and I is the moment of inertia.

Microhardness measurements of the samples were carried out as $HV_{0.5}$ from Vickers hardness type. $HV_{0.5}$ measurements were performed with QNESS GmbH Q30 M brand/model microhardness measuring device. The hardness values were determined by calculating the

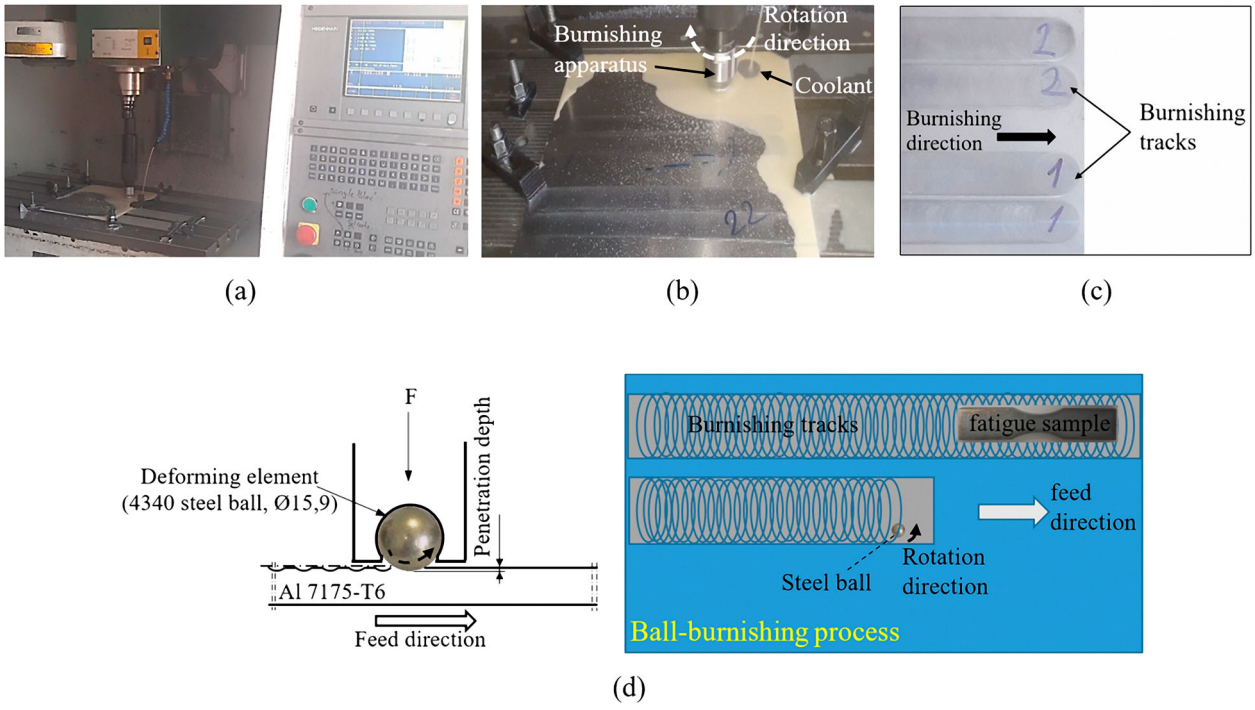


Figure 1. (a) CNC vertical machining centre, (b) burnishing, (c) burnished plate, (d) schematic representation of the burnishing process [24].

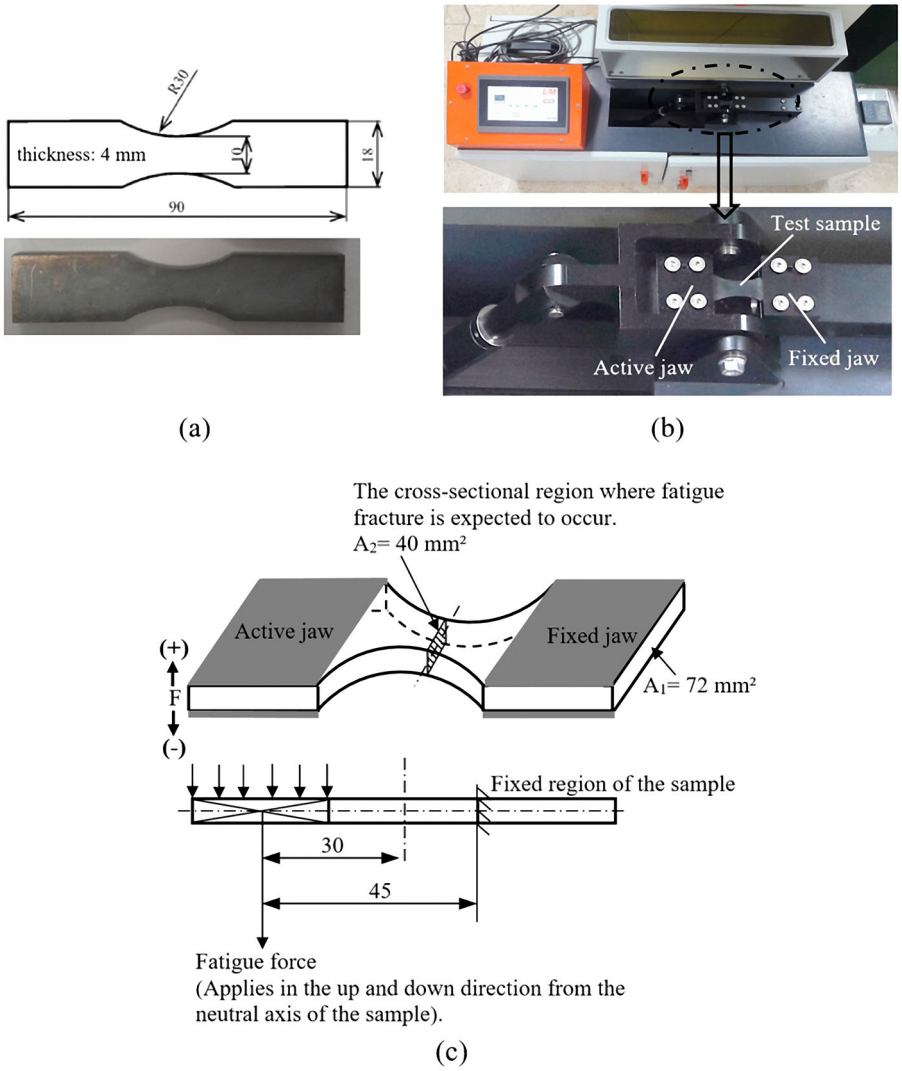


Figure 2. (a) Fatigue test sample, (b) bending fatigue tester, (c) specimen modelled as a straight beam [24].

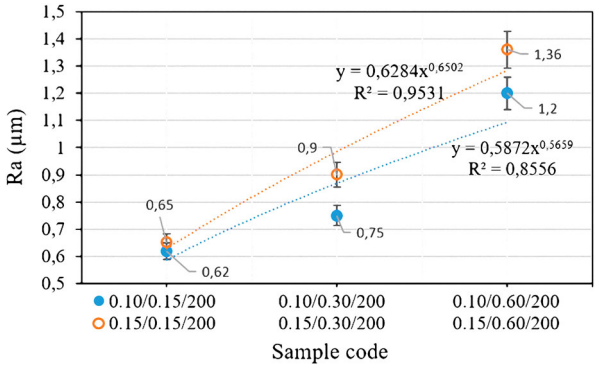


Figure 3. Effect of feed rate and penetration depth on surface roughness.

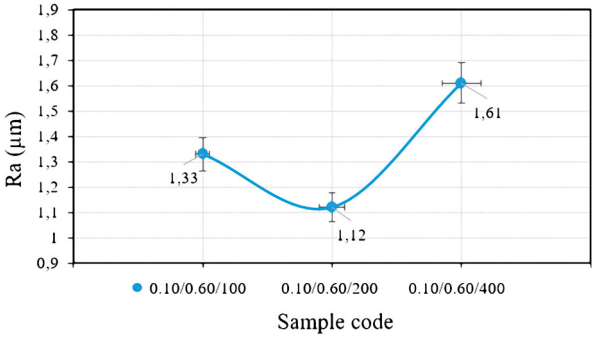


Figure 4. Effect of rotational speed on surface roughness.

arithmetic average of the five hardness measurement values taken from the burnished surfaces.

Result and discussion

Surface roughness (Ra)

In the burnishing process, the penetration depth, feed rates and rotational speed are variable parameters. Depending on these parameters, significant differences were determined in the Ra of the samples. In Figure 3, the graph showing the effect of feed rate and penetration depth on the Ra is given. The Ra value of the samples before the burnishing process is 0.39 µm.

The feed rate was implemented as 0.15–0.30–0.60 mm rev $^{-1}$. It was determined that the Ra increased with increasing feed rate (Figure 3). With the increasing feed rate, the crushing distance in each revolution increases and as a result, the Ra value increases. It is seen that there is a nearly linear increase in Ra in proportion to the increasing feed rate at different penetration depths. This result is in accordance with conventional chip removal (machining) processes. The burnishing process is a surface rolling (crushing) process and there is no material (chipping) removal from the surface. However, the Ra realities stated in the literature for conventional machining techniques are also valid in the burnishing process. Although the feed rate and rotational speed were kept constant, the increase in the penetration depth parameter negatively affected the Ra (Figure 3). The increase in the groove depth of the traces formed on the surface with the increasing penetration depth can be said to be the reason for this increase in the Ra. In addition, increasing the feed rate with increasing penetration depth negatively affected the Ra.

In Figure 4, the effect of increasing rotational speed on the Ra is given. To determine the effect of rotational speed on the Ra, the penetration depth was kept constant as 0.10 mm and the feed rate as 0.60 mm rev $^{-1}$. When the rotational speed was increased from 100 to 200 rev min^{-1}, the Ra value decreased from 1.33 to 1.12 µm, that is, the Ra value improved by about 15%. Since the increase in the rotational speed will cause the ball to pass from the same point with more repetitions in the feed distance, the Ra will improve with increasing rotational speed. However, as a result of increasing the rotational speed from 200 to 400 rev min^{-1}, an approximately 43% increase in the Ra value occurred. In the burnishing process, regional cold deformation occurs on the surface. The increase in the rate of cold deformation with the increase in rotational speed and the fact that the crushing ball causes scraping on the surface can be said to be the reason for this increase in Ra. The penetration depth, feed rate and rotational speed are the burnishing process parameters. These parameters affect the rate of cold deformation that will occur at the surface and near the surface. Increasing the compressive force applied to the Al sheet with increasing penetration depth increases the cold deformation rate. The cold deformation rate decreases as the distance between the crush lines formed by the ball on the plate surface increases with the increasing feed rate. Increasing rotation speed has the effect of increasing the cold deformation rate. Because with increasing rotational speed, the number of passes of the crushing ball from a point on the plate increases. In addition, the scraping effect of the crushing ball cannot be ignored in the burnishing process. When the burnishing process parameters are considered together, increasing penetration depth, feed rate and decreasing rotational speed cause scraping on the plate surface. Scraping on the surface reduces the rate of cold deformation. Because scraping on the surface acts as a chip-removal process.

Fatigue life

In Figure 5, the graph showing the effect of penetration depth on fatigue life in the burnishing process is given. When the graph is examined, the base material indicated the lowest fatigue life values for all stress values. It was observed that the fatigue life of the samples, which were burnished, increased with the varying depth of penetration. In terms of fatigue life, the samples showed similar trends. The best fatigue life values at low-stress values were given by samples with a penetration depth of 0.15 mm. In high-stress values, the

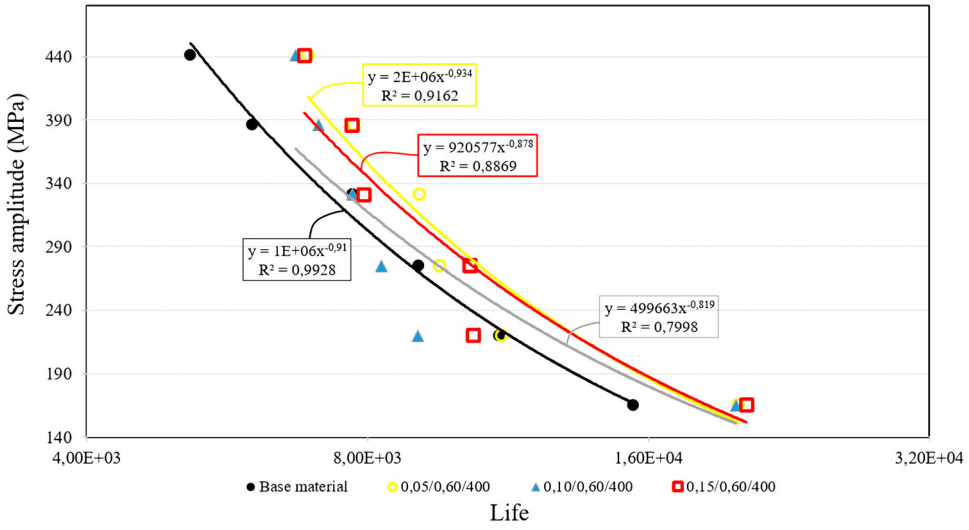


Figure 5. Effect of penetration depth on fatigue life.

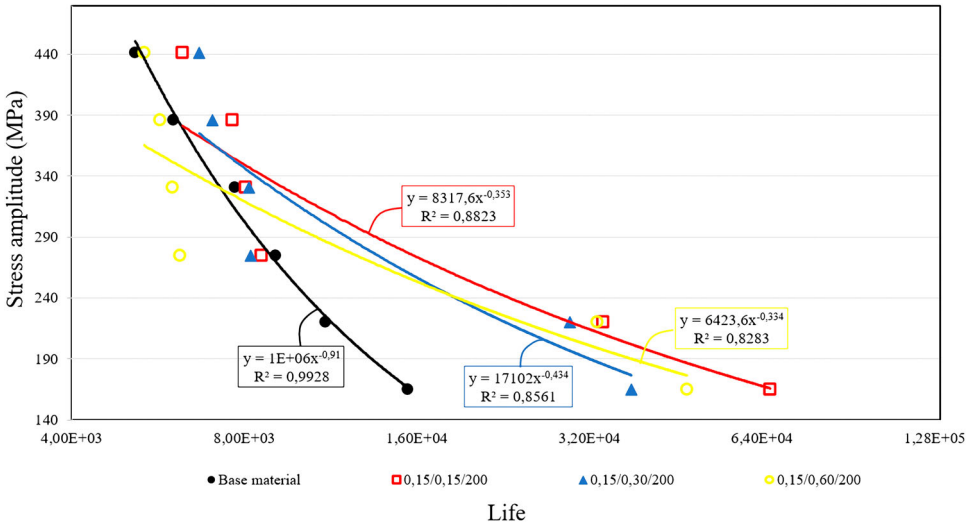


Figure 6. Effect of feed rate on fatigue life.

samples that were burnished with a penetration depth of 0.05 mm indicated the best fatigue life values. However, the difference between the samples applied with a penetration depth of 0.15 mm is only 0.9%. Therefore, while the other parameters were constant, optimum results in terms of fatigue life were obtained at a penetration depth of 0.15 mm.

In Figure 6, the effect of feed rate on fatigue life in the burnishing process is given. The base material has exhibited the lowest fatigue life values. Significant increases in fatigue life of other samples were obtained. Different roughness values on the surface depending on the feed rates caused differences in the fatigue life of the burnishing samples. When Figure 3 is examined, it is seen that while the other parameters are constant, the Ra value increases with increasing feed rates. The increase in the Ra causes both the inability to create the desired compressive stresses and the increase in the stress value locally accumulated on the surface. As a result of this, fatigue life is reduced. Therefore, the sample with the lowest feed rate of 0.15/0.15/200 indicated the best fatigue life values. Optical microstructure images of 0.15/0.15/200, 0.15/0.30/200 and 0.15/0.60/200 samples are given in Figure 7. If the burnishing surfaces are examined from the micrographs, it is seen that the 0.15/30/200 sample and the 0.15/60/200 sample have more intricate surfaces depending on the feed rate. The fatigue life of these samples is lower than that of the 0.15/0.15/200 sample since the indentations and protrusions on the surfaces cause stress concentration.

In Figure 8, the effect of rotational speed on fatigue life is given while other parameters are constant in the burnishing process. Similar to other fatigue life graphs, the base material indicated the lowest fatigue life values with varying stress values. The fatigue life of the samples increased with the burnishing process. Rotational speeds of 100–200–400 rev min^{-1} indicated similar trending fatigue life curves. The best fatigue life data were acquired by burnishing specimens with a rotational speed of 200 rev min^{-1}. The samples with the lowest fatigue life data are those surface rolled at a

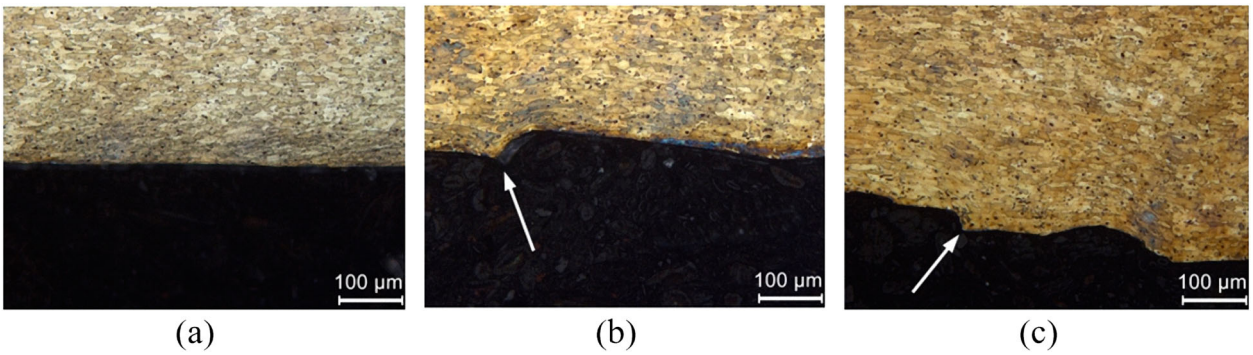


Figure 7. Optical micrographs, (a) 0.15/0.15/200, (b) 0.15/0.30/200, (c) 0.15/0.60/200.

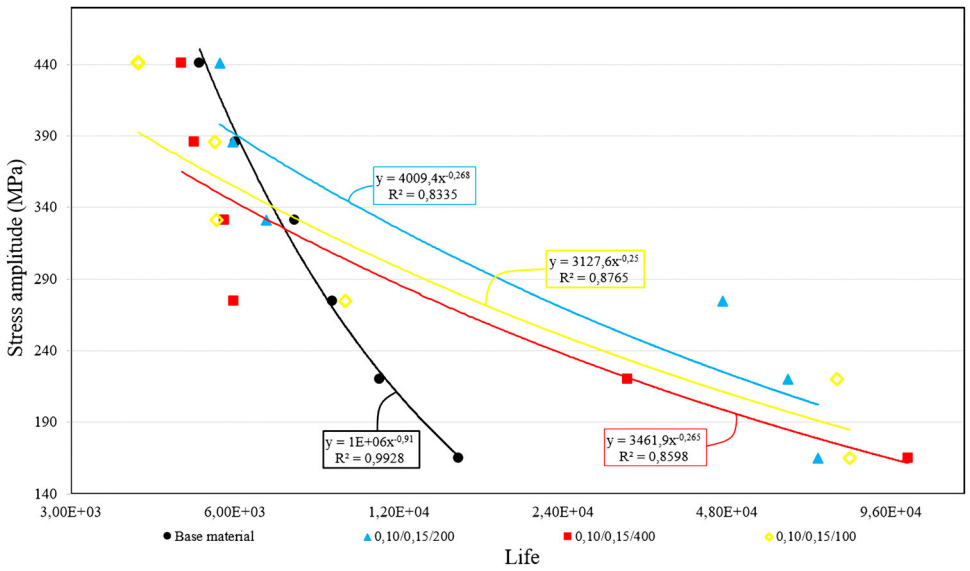


Figure 8. Effect of rotational speed on fatigue life.

rotational speed of 400 rev min^{-1}. When the graph of the effect of rotational speed on the Ra given in Figure 4 is examined, the samples that give the best and worst Ra values are the samples that were burnished with a rotational speed of 200 and 400 rev min^{-1}, respectively. Therefore, the effects of increasing rotational speed on Ra and fatigue life are similar while other parameters are constant.

As a result, when all fatigue graphs were examined, the base material exhibited the lowest fatigue life values with varying stress values. Significant increases in fatigue life were obtained in burnished samples. The fatigue life increases of the samples are associated with the Ra of the burnishing surface and the residual compressive stresses formed on these surfaces [17,23,34–36]. The improvement of the surface Ra will reduce the local stress concentrations on the surface thus preventing the formation of fatigue cracks. Residual compressive stresses formed on the surface delay the formation of cracks on the surface and/or slow down the progression rate of the crack formed. These effects lead to an increase in fatigue life. Because the effective factor in the formation of

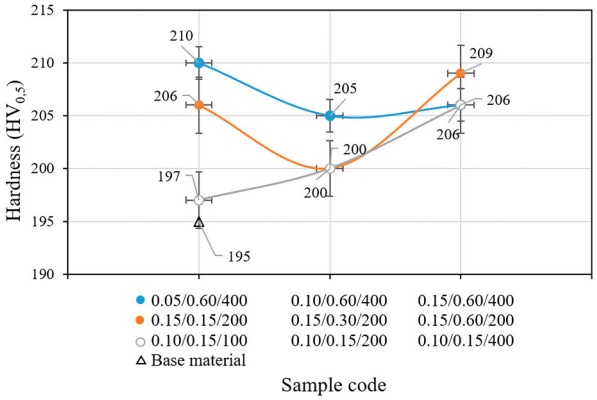


Figure 9. Microhardness measurement results.

fatigue cracking is the formation of regional stress concentrations on the surface and the regional stress value exceeding the yield stress value. Although the fatigue life of the burnished samples was higher than the base metal, the fatigue life of the samples in this study was lower than 1e5. The fatigue limit for non-ferrous alloys is specified in the literature as 2e6–2e8 [37–42]. Owing to aging heat treatment applied to

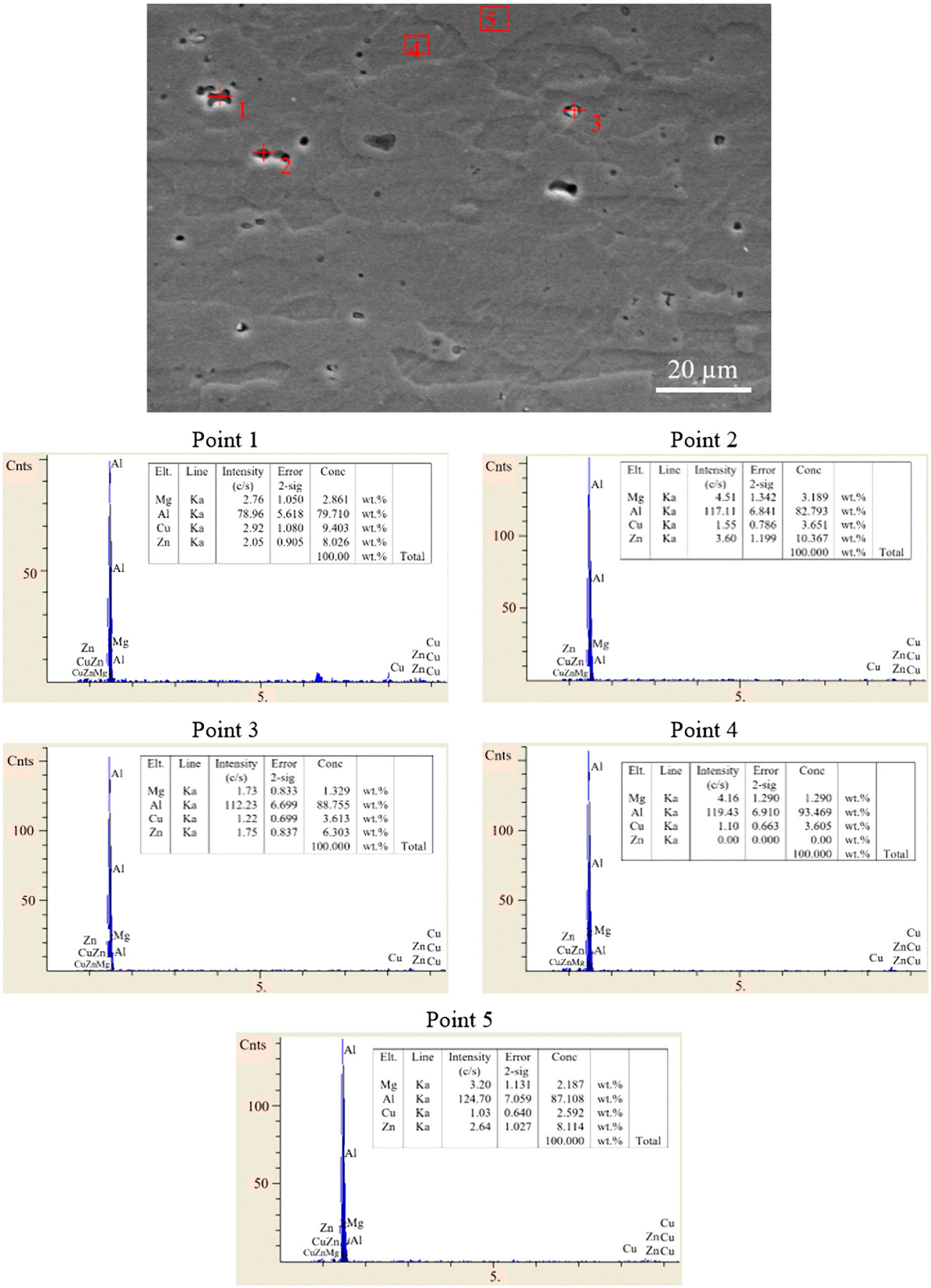


Figure 10. EDS spot analysis results of Al 7175-T6.

Al7175-T6 alloy, there are intermetallic secondary phases containing Al–Mg–Cu–Zn in its microstructure. The low fatigue life values are attributed to the fact that these phases cause a notch effect during the fatigue tests and hence the fatigue crack initiation point.

Evaluation of hardness results

The hardness of the samples was determined as microhardness from Vickers hardness type with 500 g load. Measurements were taken from the burnished surface of each sample and the arithmetic mean of

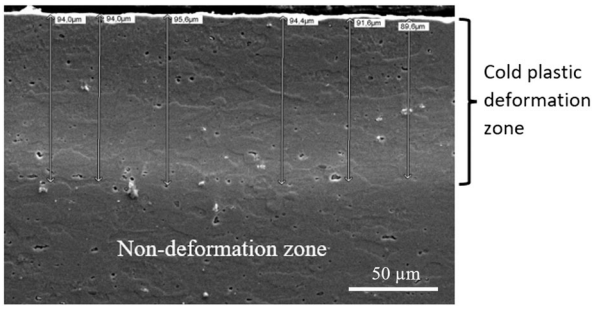


Figure 11. SEM image of 0.15/0.60/400 sample.

these measurements was calculated. The microhardness measurement results of the samples are given in Figure 9. In all samples, the hardness value is higher than the hardness value of the base material. The increase in the hardness values of the samples with burnishing is attributed to the cold plastic deformation that occurs on the surface during the process. Because the cold plastic deformation on the surface causes the grains to be oriented and the number of dislocations to increase. However, hardness values close to each other were obtained in all samples. The determined maximum hardness difference is limited to 13 $HV_{0.5}$. Therefore, it can be said that the burnishing process does not cause significant hardness changes on the surface. In fact, hardness has a significant effect on fatigue strength. Fatigue resistance increases as the hardness increases. However, the burnishing process did not cause a significant effect on the hardness value of the Al 7175-T6 alloy. For this reason, it can be said that the Ra and compressive stresses on the surface are more effective than hardness on the fatigue life values of the samples. Considering and examining Figures 5, 6, and 8 (strength-life graphs, hardness graph), it can be said that the base material has the lowest fatigue strength.

Microstructure examination

In Figure 10, point energy-dispersive spectrometry (EDS) analysis results of Al 7175-T6 material obtained in SEM are given. When the analysis results of points 1, 2 and 3 were examined, it was determined that the particles indicated by these points contained different amounts of Al–Mg–Cu–Zn by weight. Therefore, it can be said that the particles shown by these three points are different Al–Mg–Cu–Zn alloys. It has been stated in the literature that $MgZn_2$, Mg_2Zn_{11}, $Al_2Mg_3Zn_3$, Al_8Mg_5, Mg_3Zn, $CuAl_2$ and Al_2CuMg phases exist in the microstructure of the Al 7175 alloy [43–45]. Points 4 and 5 show grains that respond differently to the etching process and exist in the form of elevations and pits in the microstructure. The grains marked as 4 in the microstructure and imaged as pits are the grains that do not contain Zn according to the EDS data. The grains containing Zn were imaged as elevations in the microstructure (point 5).

SEM image of 0.15/0.60/400 sample is given in Figure 11. It was determined that the microstructural depth affected by the burnishing process was approximately 94 µm from the surface. Owing to the cold plastic deformation caused by the burnishing process, the internal energy of this region has increased and it reacted differently to Keller's reagent, creating a contrast difference.

The effect of the rotation motion of the steel ball on the orientation of the grains in the material microstructure during burnishing is given in Figure 12. Orientation and shape changes in the grains are observed with the penetration depth, feed rate, rotational speed and ball movement. This rotational effect caused by the steel ball with the burnishing process contributed to the change in the aspect ratios of the grains in the microstructure.

Conclusion

The results of this experimental study on burnishing are summarised below.

(1) The increasing feed rate in the burnishing process caused a linear increase in surface roughness.

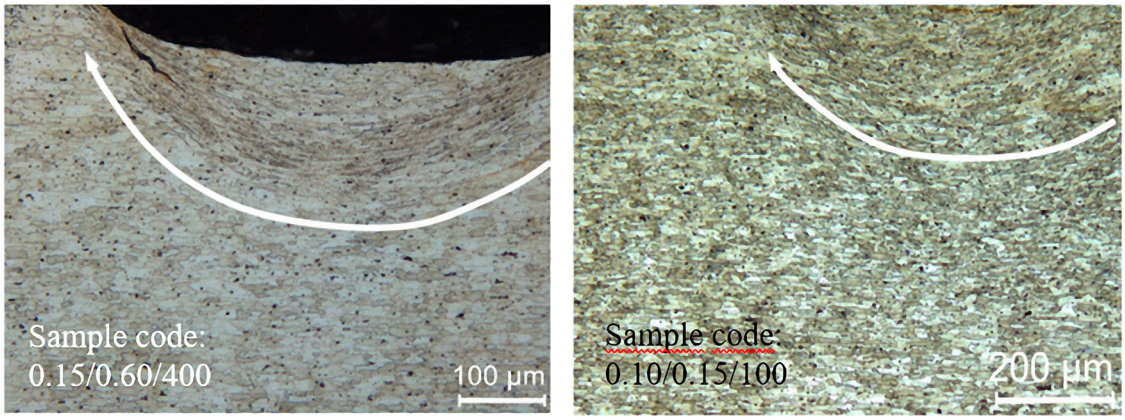


Figure 12. The effect of steel ball rotational motion on the orientation of the grains in the microstructure with the burnishing process.

(2) While the feed rate and rotational speed were stable, the increase in penetration depth negatively affected surface roughness in the burnished samples.
(3) In the burnishing process, while the penetration depth and rotation speed were stable, the fatigue life decreased with increasing feed rate. Significant increases were obtained in the fatigue life of the burnished specimens compared to the base material.
(4) The hardness value of the burnished samples is higher than the hardness value of the base material. The increase in the hardness values of the burnished samples is attributed to the cold plastic deformation that occurs on the surface during the burnishing process.
(5) According to the results of the base material EDS analysis, particles containing different wt-% Al–Mg–Cu–Zn were determined. The grains containing Zn were determined in the microstructure as elevation.
(6) In the burnishing process, the feed rate, penetration depth, rotational speed and rotational motion of the steel ball caused the aspect ratios of the grains to change in the microstructure of the burnished samples.

Disclosure statement

No potential conflict of interest was reported by the author(s).

Funding

This work has been supported by Gazi University Scientific Research Projects Coordination Unit [project number 07/2019-21, project ID 6349].

ORCID

Melika Ozer http://orcid.org/0000-0003-1807-3585
Kübra Dalli http://orcid.org/0000-0002-6335-9091
Alpay Ozer http://orcid.org/0000-0001-8496-0305

References

[1] Zhen-yu Z, Qiu-yang Z, Cong D, et al. Effect of surface burnishing process with different strain paths on the copper microstructure. J Manuf Process. 2021;71:653–668. doi:10.1016/j.jmapro.2021.09.058.
[2] Altenberger I. Deep rolling-the past, the present and the future. 9th International Conference on Shot Peening (ICSP9) 2005;144–155.
[3] Maximov JT, Anchev AP, Dunchev VP, et al. Effect of slide burnishing basic parameters on fatigue performance of 2024-T3 high-strength aluminium alloy. Fatigue Fract Eng Mater Struct. 2017;40:1893–1904. doi:10.1111/ffe.12608.
[4] Duncheva GV, Maximov JT, Dunchev VP, et al. Improvement in fatigue performance of 2024-T3 Al alloy via single toroidal roller burnishing. JMEPEG. 2021;30:2256–2266. doi:10.1007/s11665-021-05535-4.
[5] Tugay IO, Hosseinzadeh A, Yapici GG. Hardness and wear resistance of roller burnished 316L stainless steel. Mater Today-Proc. 2021;47:2405–2409. doi:10.1016/j.matpr.2021.04.363.
[6] Borysenko D, Welzel F, Karpuschewski B, et al. Simulation of the burnishing process on real surface structures. Prec Eng. 2021;68:166–173. doi:10.1016/j.precisioneng.2020.12.004.
[7] Krahmer DM, Polvorosa R, de Lacalle LNL, et al. Alternatives for specimen manufacturing in tensile testing of steel plates. Exp Tech. 2016;40:1555–1565. doi:10.1007/s40799-016-0134-5.
[8] Hassanifard S, Mousavi H, Farahani AV. The influence of low-plasticity burnishing process on the fatigue life of friction-stir-processed Al 7075-T6 samples. Fatigue Fract Eng Mater Struct. 2019;42:764–772. doi:10.1111/ffe.12950.
[9] Barahate V, Govande AR, Tiwari G, et al. Parameter optimization during single roller burnishing of AA6061-T6 alloy by design of experiments. Mater Today-Proc. 2022;50:1967–1970. doi:10.1016/j.matpr.2021.09.328.
[10] El-Khabeery MM, El-Axir MH. Experimental techniques for studying the effects of milling roller-burnishing parameters on surface integrity. Int J Mach Tools Manuf. 2001;41(12):1705–1719. doi:10.1016/S0890-6955(01)00036-0.
[11] Başak H, Göktaş HH. Burnishing process on Al-alloy and optimization of surface roughness and surface hardness by fuzzy logic. Mater Design. 2009;30(4):1275–1281. doi:10.1016/j.matdes.2008.06.063.
[12] Zhao J, Liu Z, Liang G, et al. Characterization of microstructure and mechanical properties for Ti-6Al-4V processed by rotary ultrasonic roller burnishing. Mater Charact. 2021;178:111288, doi:10.1016/j.matchar.2021.111288.
[13] Bruijn AC, GOmez-Gras G, Perez MA. On the effect upon the surface finish and mechanical performance of ball burnishing process on fused filament fabricated parts. Additive Manuf. 2021;46:102133, doi:10.1016/j.addma.2021.102133.
[14] Balland P, Tabourot L, Degre F, et al. Mechanics of the burnishing process. Prec Eng. 2013;37:129–134. doi:10.1016/j.precisioneng.2012.07.008.
[15] Rahman MA, Rahman M, Kuma AS. Chip perforation and 'burnishing – like' finishing of Al alloy in precision machining. Prec Eng. 2017;50:393–409. doi:10.1016/j.precisioneng.2017.06.014.
[16] Kovacs ZF, Viharos ZJ, Kodacsy J. Improvements of surface tribological properties by magnetic assisted ball burnishing. Surf Coat Tech. 2022;437:128317, doi:10.1016/j.surfcoat.2022.128317.
[17] Han K, Tan L, Yao C, et al. Studies on the surface characteristics of Ti60 alloy induced by turning combined with ball burnishing. J Manuf Process. 2022;76:349–364. doi:10.1016/j.jmapro.2022.02.019.
[18] Korzynski M, Lubas J, Swirad S, et al. Surface layer characteristics due to slide diamond burnishing with a cylindrical-ended tool. J Mater Process Tech. 2011;211:84–94. doi:10.1016/j.jmatprotec.2010.08.029.
[19] Lee SSG, Tam SC, Loh NH, et al. An investigation into the ball burnishing of an AISI 1045 freeform surface. J Mater Process Tech. 1992;29:203–211. doi:10.1016/0924-0136(92)90435-U.
[20] Klocke F, Liermann J. Roller burnishing of hard turned surface. Int J Mach Tools Manufact. 1998;38(5–6):419–423. doi:10.1016/S0890-6955(97)00085-0.

[21] Sönmez F, Başak H, Baday Ş. Analysis of burnishing process with response surface method. G.U J Sci Part:C. 2016;4(4):275–283.
[22] El-Axir MH, El-Khabeery MM. Influence of orthogonal burnishing parameters on surface characteristics for various materials. J Mater Process Tech. 2003;132(1–3):82–89. doi:10.1016/S0924-0136(02)00269-8.
[23] Sunny S, Mathews R, Yu H, et al. Effects of microstructure and inherent stress on residual stress induced during powder bed fusion with roller burnishing. Int J Mech Sci. 2022;219:107092, doi:10.1016/j.ijmecsci.2022.107092.
[24] Dalli K, Özer M, Yılmaz T, et al. The effect of feed speed on surface roughness and fatigue strength in burnishing process applied to Al 7175-T6 alloy. 3rd Int. Baku Scientific Research Cong. (2021):1043–1050.
[25] Esme U. Use of grey based Taguchi method in ball burnishing process for the optimization of surface roughness and microhardness of AA 7075 aluminum alloy. Adv Mat Res. 2010;44:129–135.
[26] Maximov JT, Anchev AP, Duncheva GV, et al. Impact of slide diamond burnishing additional parameters on fatigue behaviour of 2024-T3 Al alloy. Fatigue Fract Eng Mater Struct. 2019;42:363–373. doi:10.1111/ffe.12915.
[27] Huuki J, Ullah R, Laakso S. Process limitation of ultrasonic burnishing for commercially available martensitic stainless steel. Proc Manuf. 2020;51:885–889. doi:10.1016/j.promfg.2020.10.124.
[28] Rodriguez A, de Lacalle LNL, Pereira O, et al. Isotropic finishing of austempered iron casting cylindrical parts by roller burnishing. Int J Adv Manuf Technol. 2020;110:753–761. doi:10.1007/s00170-020-05894-7.
[29] Charandabi FK, Hamid RJ, Soheil M, et al. Modification of microstructure, hardness, and wear characteristics of an automotive-grade Al-Si alloy after friction stir processing. J Adhes Sci Technol. 2021;35(23):2696–2709. doi:10.1080/01694243.2021.1898858.
[30] Jandaghi MR, Pouraliakbar H, Khalaj G, et al. Study on the post-rolling direction of severely plastic deformed aluminum-manganese-silicon alloy. Arch Civ Mech Eng. 2016;16(4):876–887. doi:10.1016/j.acme.2016.06.005.
[31] Paulisch MC, Lentz M, Wemme H, et al. The different dependencies of the mechanical properties and microstructures on hot extrusion and artificial aging processing in case of the alloys Al 7108 and Al 7175. J Mater Process Tech. 2016;233:68–78. doi:10.1016/j.jmatprotec.2016.02.012.
[32] Cheong MFL, Rouse JP, Hyde CJ, et al. The prediction of isothermal cyclic plasticity in 7175-T7351 aluminium alloy with particular emphasis on thermal ageing effects. Int J Fatigue. 2018;114:92–108. doi:10.1016/j.ijfatigue.2018.05.010.
[33] Song RG, Zhang QZ. Heat treatment optimization for 7175 aluminum alloy by genetic algorithm. Mater Sci Eng: C. 2001;17(1–2):133–137. doi:10.1016/S0928-4931(01)00321-6.
[34] Egea AJS, Rodriguez A, Celentano D, et al. Joining metrics enhancement when combining FSW and ball-burnishing in a 2050 aluminium alloy. Surf Coat Technol. 2019;367:327–335. doi:10.1016/j.surfcoat.2019.04.010.
[35] Rodriguez A, Calleja A, de Lacalle LNL, et al. Burnishing of FSW aluminum Al–Cu–Li components. Metals (Basel). 2019;9:260, doi:10.3390/met9020260.
[36] Huang B, Kaynak Y, Sun Y, et al. Surface layer modification by cryogenic burnishing of Al 7050-T7451 alloy and validation with FEM-based burnishing model. Proc CIRP. 2015;31:1–6. doi:10.1016/j.procir.2015.03.097.
[37] Azar RG, Parast MSA, Azadi M. Heat-treating and nano-reinforcing improvements on fretting fatigue properties and fracture behaviors of cylinder head aluminum alloys. J Mater Res Technol. 2022;20:1927–1939. doi:10.1016/j.jmrt.2022.08.002.
[38] Xu S, Chena J, Shen W, et al. Fatigue strength evaluation of 5059 aluminum alloy welded joints considering welding deformation and residual stress. Int J Fatıgue. 2022;162:106988, doi:10.1016/j.ijfatigue.2022.106988.
[39] Tianyu Z, Teng Z, Yuting H, et al. Probabilistic model of the fatigue life of epoxy-coated aluminum alloys considering atmospheric exposure. Int J Fatıgue. 2022;162:106899, doi:10.1016/j.ijfatigue.2022.106899.
[40] Kapidžić Z. Comparison of fatigue life and flexibility between aluminum-composite and aluminum–aluminum bolted joints. Int J Fatıgue. 2022;157:106695, doi:10.1016/j.ijfatigue.2021.106695.
[41] Zobaer Shah QM, Chowdhury MA, Kowser MA. The aspect of the corrosion pitting with fretting fatigue on aluminum alloy: an aerospace structural failure or a nuclear safety phenomenon. Results Eng. 2022;15:100483, doi:10.1016/j.rineng.2022.100483.
[42] Liu Y, Pan Q, Liu B, et al. Effect of aging treatments on fatigue properties of 6005A aluminum alloy containing Sc. Int J Fatıgue. 2022;163:107103, doi:10.1016/j.ijfatigue.2022.107103.
[43] Banhart J. Age hardening of aluminum alloys. In: GE Totten, editor. ASM handbook volume 4E: heat treating of nonferrous alloys. ASM International; 2016. p. 214–239. doi:10.31399/asm.hb.v04e.a0006268.
[44] Panait N, Ciurdas M, Stephan R. Microstructural characterization of AA-7175 alloy slabs. U.P.B Sci Bull Series B. 2009;71(2):93–101.
[45] Lim ST, Eun IS, Nam SW. Control of equilibrium phases (M,T,S) in the modified aluminum alloy 7175 for thick forging applications. Mater Trans. 2003;44(1):181–187. doi:10.2320/matertrans.44.181.